Available online at www.sciencedirect.com
SCIENCE DIRECT®
International Journal of Mass Spectrometry 230 (2003) 99–112
International Journal of Mass Spectrometry
www.elsevier.com/locate/ijms

Mass spectrometric determination of the ionisation cross-sections of BaO, Ba, BaF_2 and BaI_2 by electron impact

Arkadij Popovič*

Jozef Stefan Institute, Jamova 39, 1000 Ljubljana, Slovenia

Received 8 April 2003; accepted 31 July 2003

Abstract

A Nier-type mass spectrometer coupled with a Knudsen cell was used for the ionisation cross-section measurements of Ba, BaO, BaF_2 and BaI_2, using appropriate internal standards with known ionisation cross-sections. The vapour pressure ratio of standard to investigated compound, needed for calculation was obtained via the chemical analysis of the effusate. The use of this approach eliminated several sources of uncertainties. The problems concerning the preferential loss of fragment ions was also discussed and partly eliminated. The results obtained were compared with predictions, usually used in the field of high temperature mass spectrometry and a more recent approach using a model for ionisation cross-sections of high temperature molecules (MCM).

Keywords: Ionisation cross-section; Knudsen cell; Barium oxide; Vapour pressure

1. Introduction

The outstanding importance of barium oxide in the electronic and lamp industries inspired a number of researchers to study its evaporation thermodynamics using various methods starting with Langmuir evaporation in the early work of Thompson in 1829. More recently, the vapour pressure of BaO was determined by Hilpert et al. in 1974 using Knudsen effusion combined with mass spectrometry (KCMS). Considering the results obtained by different authors one realises that regardless of the method applied the resulting vapour pressure of BaO is surprisingly consistent (Table 1). To be more specific, the results obtained by KCMS agree with those obtained by other methods. It must be pointed out here, that unlike Langmuir or the Knudsen method, KCMS is not absolute since it implies the use of the ion current ratio and the ionisation cross-section ratio of the investigated compound and the standard, which is usually silver. Thus, the reliability of the measured vapour pressure directly depends on the accuracy of the ionisation cross-section of the measured compound. In most cases, this is obtained using the additive rule introduced by Otvos and Stevenson [1]. It implies the summation of atomic cross-sections (usually taken from Mann's [2] theoretical calculations), followed by arbitrary correction [3] and it is assumed that the molecular cross-sections obtained are within acceptable limits (20–30%). In the works of Inghram et al. [4], Farber and Srivastava [5] and Hilpert and Gerads [6] silver was used as a reference material with a Ag to BaO relative cross-section of 0.5, 0.57 and 0.42, respectively. Despite the different energy of the ionising electrons used by authors, they all employed a similar cross-section ratio. Considering 0.5 as a mean value and $5.4 \times 10^{-16}\,cm^2$ as the ionisation cross-section of silver we find that a value of $11.0 \times 10^{-16}\,cm^2$ was taken for the ionisation cross-section of BaO. Although, the way the authors applied the additive rule was different the fact is that all obtained a similar BaO vapour pressure, which agree with those obtained by classical evaporation methods (Table 1). Thus, the value of $11.0 \times 10^{-16}\,cm^2$ could be assumed as a reliable approximation for the ionisation cross-section of BaO. However, recently Hastie [7] introduced a novel concept into the additivity rule involving the 'ionic' instead of 'atomic' cross-sections to predict the molecular cross-sections. The model proposed that in the case of strongly ionic molecules (such as high temperature species) it is mainly the anionic part of the molecule that looses the electron by ionisation. Following the procedure described in [7] a value of $1.6 \times 10^{-16}\,cm^2$ is obtained for the

* Tel.: +386-1-4773409; fax: +386-1-2519-385.
E-mail address: arkadij.popovic@ijs.si (A. Popovič).

1387-3806/$ – see front matter © 2003 Elsevier B.V. All rights reserved.
doi:10.1016/j.ijms.2003.07.002

Table 1
Vapour pressure of BaO at 1523 K obtained by different authors using various methods

Author	Method	*p*BaO at 1523 K/atm
Claassen and Veenemanns [9]	Rate of evaporation (Langmuir experiment)	1.133E−7
Blewett et al. [10]	Knudsen evaporation; the amount of evaporate measured	1.026E−7
Newbury et al. [11]	Knudsen evaporation coupled with thermobalance	1.133E−7
Semenov et al. [12]	KCMS, isothermal total evaporation	1.251E−7
Inghram et al. [13]	KCMS, silver used as a reference	1.17E−7
Farber and Srivastava [14]	KCMS, silver used as a reference	1.021E−7[a]
Hilpert and Gerads [6]	KCMS, silver used as a reference	8.358E−8
JANAF [15]	Recalculated	1.707E−7
IVTANTHERMO [16]	Recalculated	1.371E−7

[a] Calculated from Farber's original data.

ionisation cross-section of BaO. This value was confirmed by the same author in [8] as 1.8×10^{-16} cm^2, this being the only experimental value for the ionisation cross-section of BaO obtained so far. This disagreement between the results certainly calls for the re-determination of the ionisation cross-section of BaO, which is the main objective of the present work.

2. Experimental approach

A common approach in KCMS experiments is to evaporate the substance under investigation simultaneously with a standard material (under Knudsen conditions) from a Knudsen cell, positioned in front of the ion source of the mass spectrometer. The narrow, axial part of the effusing molecular beam is admitted into the ionisation region where ions are created and further analysed by their mass number and abundance. The vapour pressure of the substance is then obtained according to Eq. (1)

$$p_x = \left(\frac{\sum I_x}{I_r}\right) \times \left(\frac{\sigma_r}{\sigma_x}\right) \times p_r \quad (1)$$

where p, σ and I refer to the pressure, ionisation cross-section and ion currents of the reference material (r) and measured compound (x). If, the relative ionisation cross-section is of interest, the relative vapour pressure (or activities) must be known. Using this approach Alcock [17] measured the relative ionisation efficiencies of Cu/In, Ni/Fe, Co/Fe, Al/Fe, Ag/Au and Cu/Ag alloys. It is obvious, however, that the reliability of the results depends on the pressures and/or the activities of the components. In the present study, the investigated material was evaporated together with the reference, but the relative pressures (p_x/p_r) have been obtained by analysing the Knudsen cell deposited material, independently form literature pressure data. To accomplish this, the condensed material was collected on Scots tape pasted on the water cooled wall of the vacuum chamber opposite the Knudsen cell. Using this approach, a number of problems can be overcome, such as vapour pressure and activity data uncertainty, questions involving evaporation and condensation coefficients and possible temperature gradients. Uneven spatial distribution of the evaporating substances (due to possible creeping) can also be ruled out since only the axial part of the molecular beam entering the ion source and is collected and thus chemically analysed. The relative vapour pressure (p_x/p_r) inside the cell can be obtained from considerations given in [18] by

$$\frac{p_x}{p_r} = \frac{n_x}{n_r} \times \sqrt{\frac{M_x}{M_r}} \quad (2)$$

here, n_x/n_r is the molar ratio of sample (x) and reference material (r) found in collected material and M is the molecular mass. A typical amount of deposited material in our experiments was within microgram range. It was removed from the tape by dissolving it in 20 μl of appropriate acid (ultra pure acids HCl, HNO_3 or aqua regia were used) and diluted with water to 2 ml an amount sufficient for analysis by inductive coupled plasma-atomic emission spectroscopy analysis (ICP-AES). A combination of Eqs. (1) and (2) gives the relative ionisation cross-sections free from all systematic errors except those introduced by discrimination effects concerning transmission of ions through the mass spectrometer. From an analytical point of view, it is desirable to use a standard with a similar vapour pressure and a well-known cross-section. In the case of BaO, gold was selected as the most appropriate as far as vapour pressure is concerned. For inter-comparison and method validation, several other systems were additionally studied such as; Au/Cu, Ba/Al, Ag/Cu, BaF_2/Cu and BaI_2/Ag.

2.1. Mass spectrometer and the ion source

2.1.1. Ion source

A 60° magnetic low resolution mass spectrometer with a modified Nier-type ion source was used. Electrons were obtained from a V-shaped tungsten cathode inside a Vehnelt cylinder and extracted through a 1.5 mm hole by a positively charged plate (+15 V with respect to the cathode) positioned 2 mm away from the cathode. The electrons were guided through the ionisation chamber to a Faraday cup (3 mm deep, 2 mm in diameter) by an axial magnetic field. The cathode current was regulated to ensure a constant electron trap current of 10 μA. The trajectories of the electrons were directed

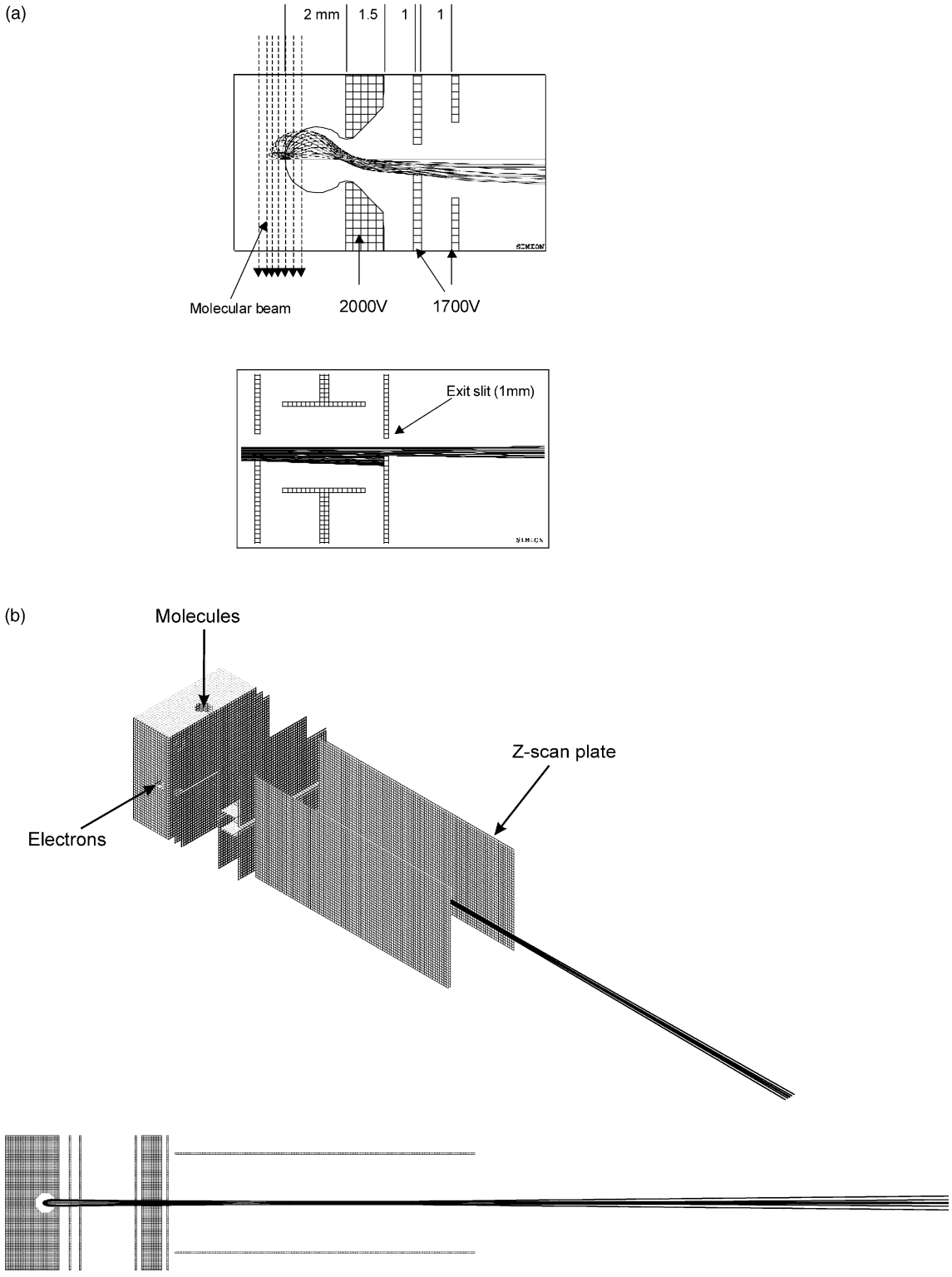

Fig. 1. (a) Top: Detail of the ion source in *X*–*Y* plane. Shown are simulated trajectories for ions with 0.7 eV kinetic energy with starting angles from 0° to 180°. Equipotential line indicates 1997.5 V. The potential gradient within the electron–molecule interaction volume is 1.5 V/mm. All ions are extracted from the ionisation chamber. Bottom: Detail of the ion source at the exit slit. Blocked are all ions with a starting angle between 15° and 120°. However, all molecular ions with energy ≤0.1 eV can pass through the exit slit. (b) Simulation of trajectories for ions with a starting angle from 0° to 360° and 0.7 eV kinetic energy. Top: 3D-view. Bottom: View in *X*–*Z* plane.

along the ion extraction slit (3 mm long, 1.5 mm wide), at a distance of 2 mm. Ions were drawn from the ion source using a penetrating field, provided by an adjustable potential extraction plate (with a slit 5 mm long by 1 mm wide) placed 1.5 mm beyond the ion extraction slit. Ions were further focused by changing the respective potential (50 V) of two semi plates, 2.5 mm apart. These plates served to focus the ion beam onto the exit slit of the ion source. This slit (the resolution defining slit) was kept unusually wide (1 mm). By setting the slit to 1 mm, we decreased the resolving power of our device to avoid artefacts in the ionisation curves and gained better transmission for more dispersed ions (energetic fragment ions). The most important feature of our ion source was that while scanning the electron energy from 6 to 100 eV the total electron emission current (20 μA) altered by less than 10%, and remained constant from 15 up to 100 eV when keeping the current of ionising electrons (trap current) constant within specified limits 10 ± 0.1 μA. It was not necessary to readjust the penetrating field strength to optimise the ion peak intensity. It was kept unchanged in all experiments (40 V), regardless of the applied electron energy. In Eq. (1) terms $\sum I_x$ and I_r represent the sum of fragment abundance originating from the molecule of interest and reference material, respectively. It was shown in several studies by Maerk and co-workers [19] and Gorokhov and Khandamirova [20], that taking simple sum for $\sum I_x$ is not adequate. It is known that fragment ions can possess a significant amount of kinetic energy. Such ions are subjected to different kinds of discrimination during their passage through the mass spectrometer. In particular, they are not extracted from the ion source with the same efficiency as are the thermal (molecular) ions. Fig. 1a shows SIMION simulation (in *XY* plane) of the extraction properties of our ion source for ions with 0.7 eV kinetic energy. While they can be all extracted from the ionisation volume, a part of them is blocked at the exit slit. Energetic ions are also preferentially lost at the magnet slit since unlike the molecular ions they are significantly dispersed in the *Z* direction (parallel to the magnet field). Fig. 1b shows simulated ion trajectories in *ZX* plane having 0.7 eV average kinetic energy. Such a divergent ion beam cannot be focused by a Nier-type of magnet to the detector and also not all the ions can pass the magnet slit (3 mm high in *Z* direction). To compensate the effects of this discrimination, Maerk and co-workers proposed scanning the ion beam over the slit using two electrodes. Gaussian-like curves are obtained and the area rather than the intensity are taken for ion abundance. From this point on we shall call those curves *Z*-scan distributions. This method was also used in the present work. Scanning was accomplished by two semi-electrodes (45 mm of length 14.5 mm apart), mounted immediately after the ion exit slit, see Fig. 1b.

It is important to note, that in KCMS experiments the sample is introduced into the ion source as a narrow beam (3 mm in diameter in our case) of neutral molecules with a thermal velocity predominantly in the *Y* direction with little or no *Z* component. After ionisation, the molecular ions retain their velocity in the *Y* direction but the fragments gain a significant portion of energy (comparing to the thermal part) in all directions. As a result, one would expect extremely narrow *Z*-scan distribution of molecular ions. In reality, the observed broadening of the molecular ions is because that they are created within the non-equipotential volume. In our experimental arrangement, a potential gradient as high as 1.5 V/mm was obtained by a SIMION calculation, within the ionisation volume. Broadening is also caused by scanning over a magnet slit of finite height (3 mm). In any case, the *Z*-scan distribution of molecular ions can easily be distinguished from fragments by being essentially narrower. Also the *Z*-scan of background molecular (thermal) ions (such as N_2, H_2O, Ar etc.) show even broader distribution than fragments of high temperature species. The reason is probably that the latter are created within a smaller volume (defined by beam cross-section) than the former.

Table 2a
Raw data from BaO–Au system

Run	Au^+	Au^{2+}	BaO^+	Ba^+	Ba/BaO
Ion intensities in counts per 0.1 s					
1	16697	2714	944	516	0.55
2	16555	2681	966	512	0.53
3	16847	2710	967	503	0.52
4	16244	2556	993	491	0.49
5	15408	2546	923	503	0.54
Average	16350	2641	959	505	0.53
Relative standard deviation (%)	3	3	3	2	4
Integrated area under the *Z*-scan (arbitrary unit)					
1	451502	64635	27530	21660	0.79
2	431992	70284	26653	21767	0.82
3	437287	69451	26846	22002	0.82
4	460685	70389	25946	22597	0.87
5	454920	69431	25842	22445	0.87
Average	447277	68838	26563	22094	0.83
Relative standard deviation (%)	2	3	3	2	4

2.1.2. Evaporator

Samples were evaporated from a cell (Ø 10 mm) with a 0.1 mm orifice. To avoid thermal gradients, the cell was embedded in a 2-mm thick Mo crucible, placed inside a

Table 2b
Double ratio for parent (Au) to fragment (Ba) ions deviates from unity by 60%

Run	$(Au^+/Au^{2+})_{int}/(Au^+/Au^{2+})_{area}$	$(Au^+/BaO^+)_{int}/(Au^+/BaO^+)_{area}$	$(Au^+/Ba^+)_{int}/(Au^+/Ba^+)_{area}$
1	0.88	1.08	1.55
2	1	1.06	1.63
3	0.99	1.07	1.69
4	0.97	0.92	1.62
5	0.92	0.95	1.51
Average	0.95	1.01	1.60

More Ba^+ ions are lost due to the divergence of Ba^+ beam.

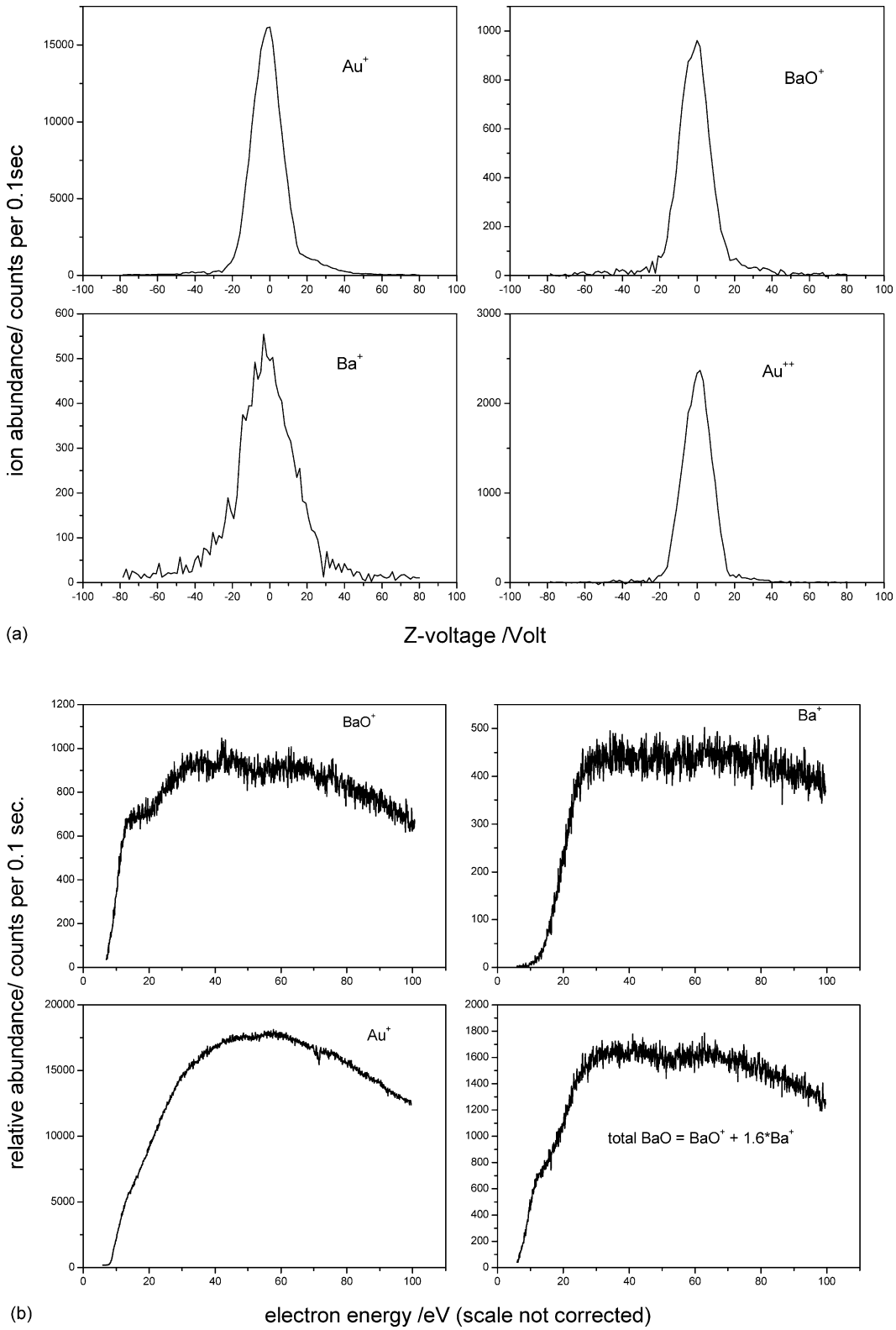

Fig. 2. (a) *Z*-scan curves for Ba^+, BaO^+ and Au^+ ions measured at 50 eV. BaO–Au system at 1523 K. Notice broader distribution of Ba^+ fragment ion in comparison with parent BaO^+ and atomic Au^+ and Au^{2+}. (b) Relative ionisation cross-section curves for Ba^+, BaO^+ and Au^+ ions. BaO–Au system at 1523 K. Total BaO is obtained by summation of the BaO^+ abundance and abundance of Ba^+, corrected by factor of 1.6.

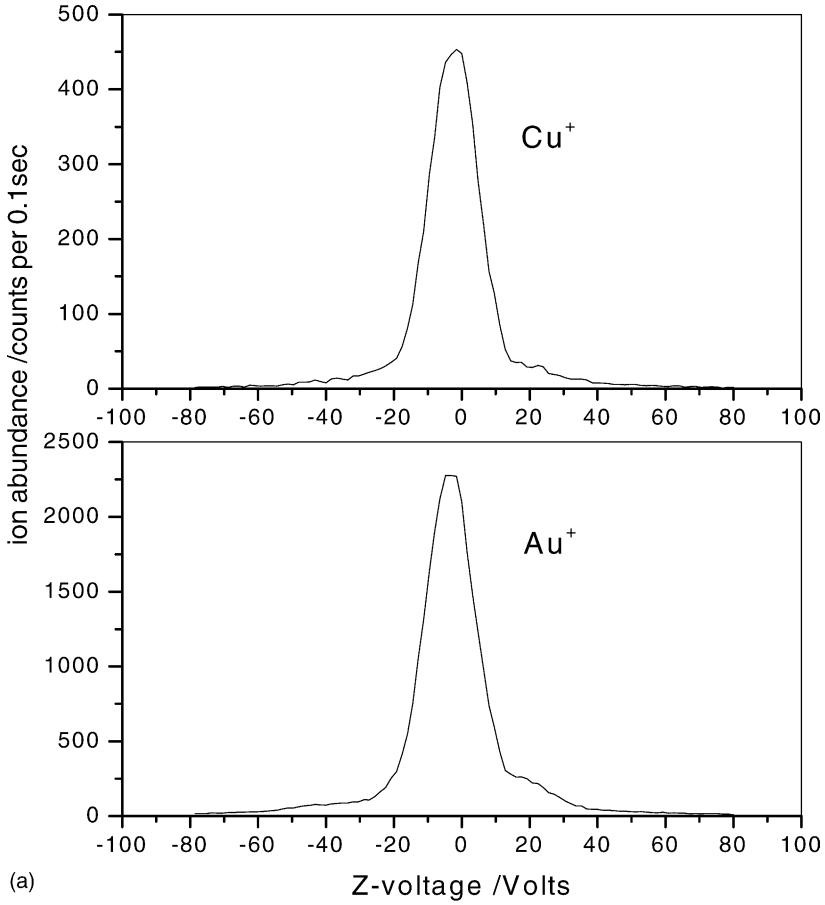

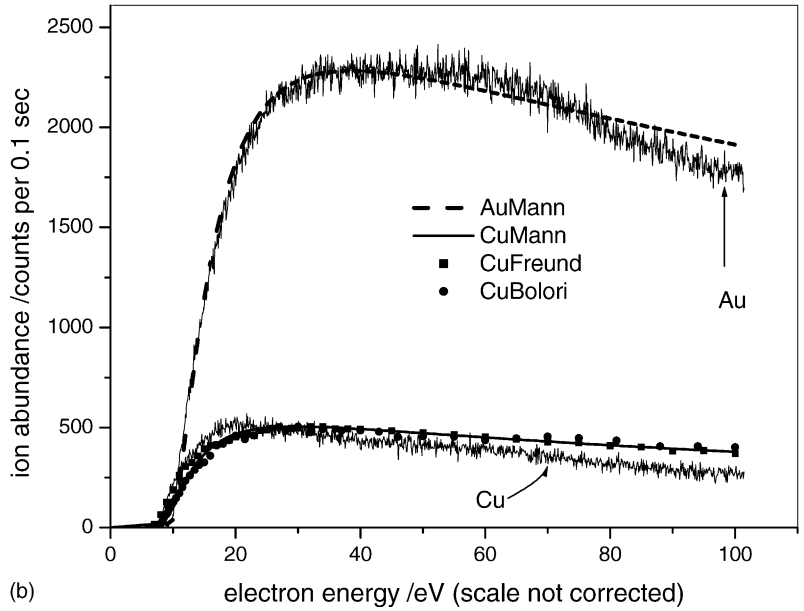

Fig. 3. (a) Z-scan curves for $^{63}Cu^{+}$ and Au^{+} measured at 1523 K and 40 eV. System Au0.53/Cu0.47 alloy. (b) Relative ionisation cross-section curves for $^{63}Cu^{+}$ and Au^{+} obtained from an Au0.53/Cu0.47 alloy at 1523 K. Also shown are the theoretical curves of Mann and experimental curves of Freund et al. [26] and Bolorizadeh et al. [27]. A perfect match could not be obtained in this case.

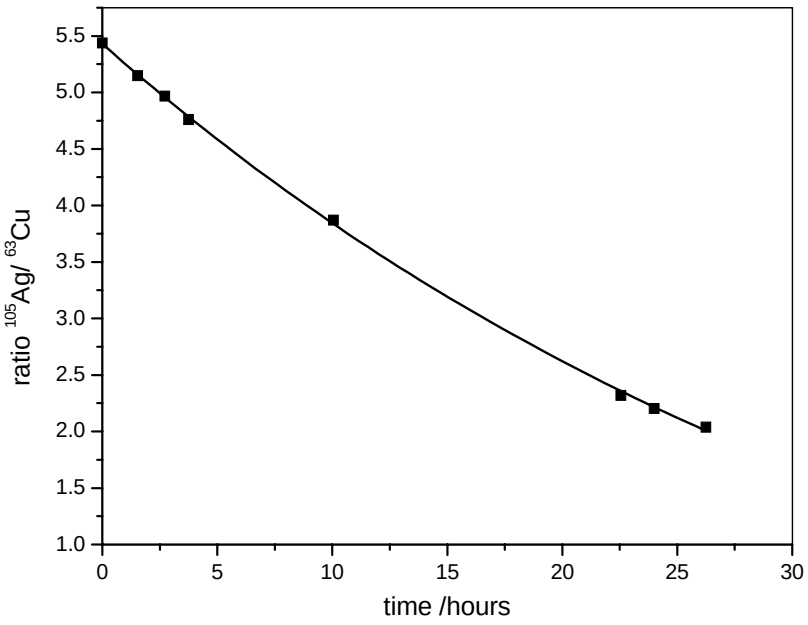

Fig. 4. $^{105}Ag^{+}/^{63}Cu^{+}$ ratio in variation with time. The calculated average ratio is 3.55.

quartz tube heated by a Mo spiral. The temperature was measured by a Pt/PtRh (10%) thermocouple (0.1 mm in diameter) spot welded to the Mo crucible, and maintained by a EUROTHERM programmable regulator at a given temperature to better than ±1 °C. Two layer tantalum radiation shields were installed around the Mo heating spiral to minimise the heat loss and thermal gradients. The distance from the cell orifice to the ion source sample entrance hole (Ø 3 mm) and the electron path was 2 and 3 cm, respectively. A 5-mm thick copper plate (with a circular opening, 3 mm in diameter) was placed between the Knudsen cell and ion source, cooled by liquid nitrogen, on which most of the effusing material condensed to prevent ion source contamination. Between this plate and the Knudsen cell, a manual operated shutter was installed, to distinguish between ions formed from background gases and ions originating from the effusing molecules. To minimise the oil background, the 'pure' vacuum was provided by a liquid nitrogen sorption pump followed by a He cryo-pump. The detector part of the analyser tube was additionally pumped by an turbomolecular pump. The typical operating pressure in the ion source region and detector region was below 10^{-7} mbar.

Ions were detected by an ETP active film electron multiplier (AF151H) operating in the counting mode using a 225 MHz HP 5315A counter. The multiplier was fed by a −3.5 kV voltage supply which is sufficient to avoid mass discrimination on the first multiplier dynode. During measurements, when the shutter was closed the counting rate was less than 10 Hz, at all *m/z* of interest.

To obtain the ionisation cross-section curves in the range from the threshold to 100 V, a scan of electron energy was made using a constant speed motor drive coupled to a 10 turn precision potentiometer, simultaneously acquiring the ion abundance at a rate of 10 points per second.

Table 3a
Raw data for a Cu–BaF_2 system

Run	Cu^+	Ba^+	BaF^+
Intensity in counts per 0.1 s			
1	18229	14234	38214
2	13698	14031	35283
3	15374	14092	35934
4	14331	11810	31446
Average	15408	13542	35219
Relative standard deviation (%)	13	9	8
Area (arbitrary unit)			
1	575646	619649	1448000
2	401221	608684	1342480
3	482016	608916	1374000
4	445769	529219	1208800
Average	476163	591617	1343320
Relative standard deviation (%)	16	7	7

Table 3b
A different value for the ratio of Ba^+ and BaF^+ indicates, that Ba^+ ions are more dispersed (gain higher kinetic energy by ionisation of BaF_2) than the BaF^+ ions

Run	$(Cu^+/Ba^+)_{int}/(Cu^+/Ba^+)_{area}$	$(Cu^+/BaF^+)_{int}/(Cu^+/BaF^+)_{area}$
1	1.379	1.200
2	1.481	1.299
3	1.378	1.220
4	1.441	1.236
Average	1.420	1.239
Relative standard deviation	3.07	3.00

3. Results

As seen in Table 1, in all cases silver was used as the reference material, which is surprising since the much higher (5000 times) vapour pressure relative to BaO prevents simultaneous measurements at the same temperature. Therefore in this work, gold was selected as better choice as far as vapour pressures are concerned. In a typical experiment 300 mg of pre-baked BaO was loaded in the alumina cell together with 100 mg of pure gold. The cell was then transferred into the mass spectrometer, evacuated and degassed for 24 h at 1273 K. The temperature was finally raised to

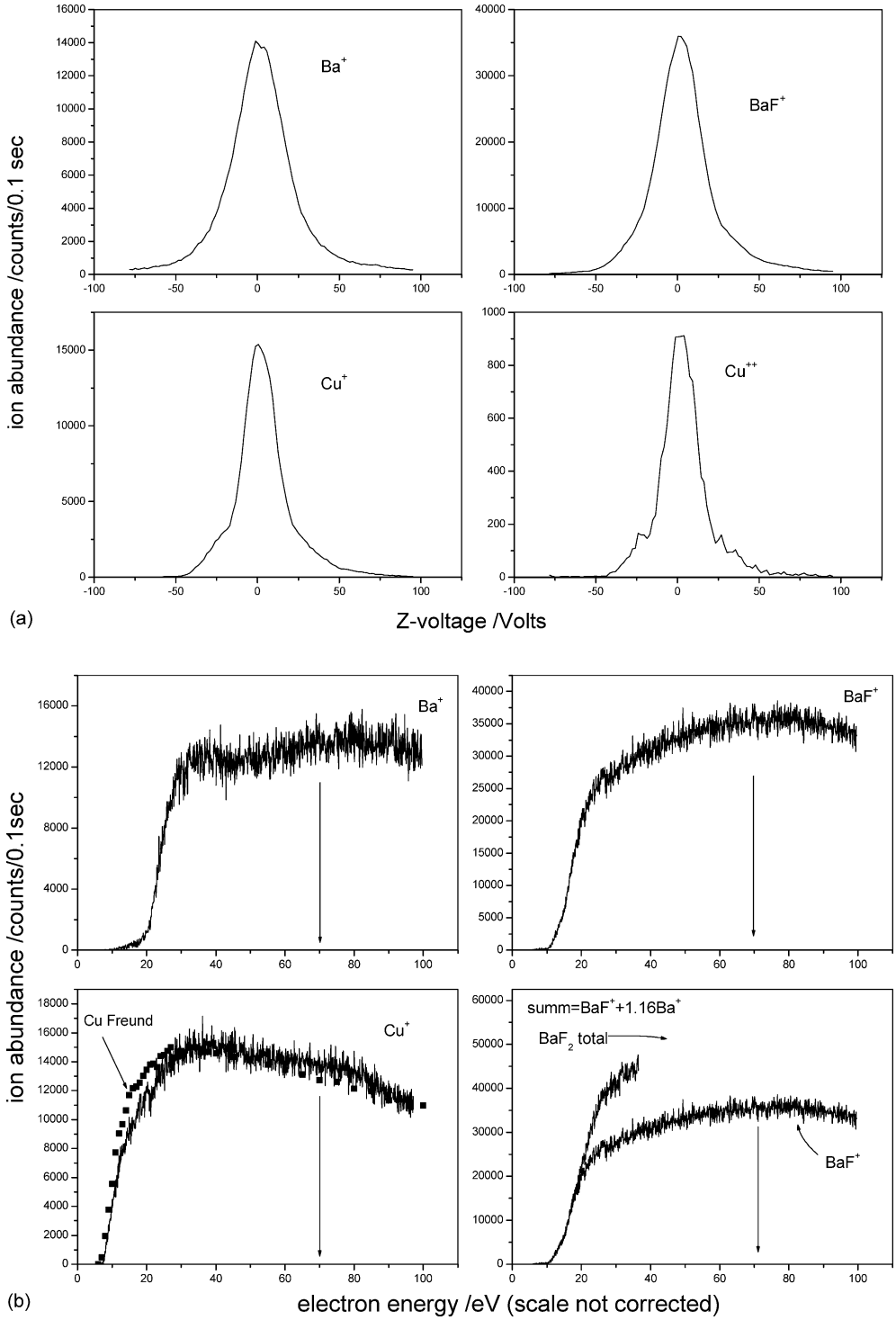

Fig. 5. (a) Cu–BaF_2 system. *Z*-scan curves measured at 70 eV. (b) Relative ionisation cross-section curves for ions obtained from Cu–BaF_2 system. Match with Freund's shape for Cu is also shown.

1523 K and kept constant for several days. During this period the ion abundance was occasionally measured by scanning the ion beam over the magnet slit in the Z direction. Only Ba^+, BaO^+, Au^+ and Au^{2+} were measured. A typical run is presented in Fig. 2a (Tables 2a and 2b).

A series of five runs were evaluated and data collected in Table 2a. Ionisation cross-section curves were also measured from 6 to 100 eV. The runs are shown in Fig. 2b. The ionisation threshold of the Ba^+ ion of about 10 eV indicates that the Ba^+ ion is a product of dissociative ionisation of BaO rather than simple ionisation of the Ba atom. The Ba^+/Ba ionisation curve appears markedly different than Ba^+/BaO (see Ba^+ curves in Figs. 5b and 8). Finally, the Ba^+/BaO^+ abundance ratio also match the ratio obtained by Hilpert and Gerads [6] measured in a non-reducing cell. From data collected in Table 2a and chemical analyses of deposited material (31.8 μg Au and 2.1 μg Ba) we obtained the ionisation cross-section of BaO using Eq. (3):

$$\sigma_{BaO} = \left(\frac{m_{Au}/M_{Au}}{m_{BaO}/M_{BaO}} \times \sqrt{\frac{M_{Au}}{M_{BaO}}} \right) \times \left(\frac{I_{BaO^+} + I_{Ba^+}}{I_{Au^+}} \right) \times \left(\frac{\eta_{Au}}{\eta_{Ba}} \right) \times \sigma_{Au} \quad (3)$$

here, m, M, I and η represent mass, molecular mass, ion abundance or area and isotope abundance correction ($\eta_{Au} = 1$, $\eta_{Ba} = 0.72$), respectively. With the supposition that $\sigma_{Au}(\max) = 5.84 \times 10^{-16}\ cm^2$ (Mann's [21] value) we get

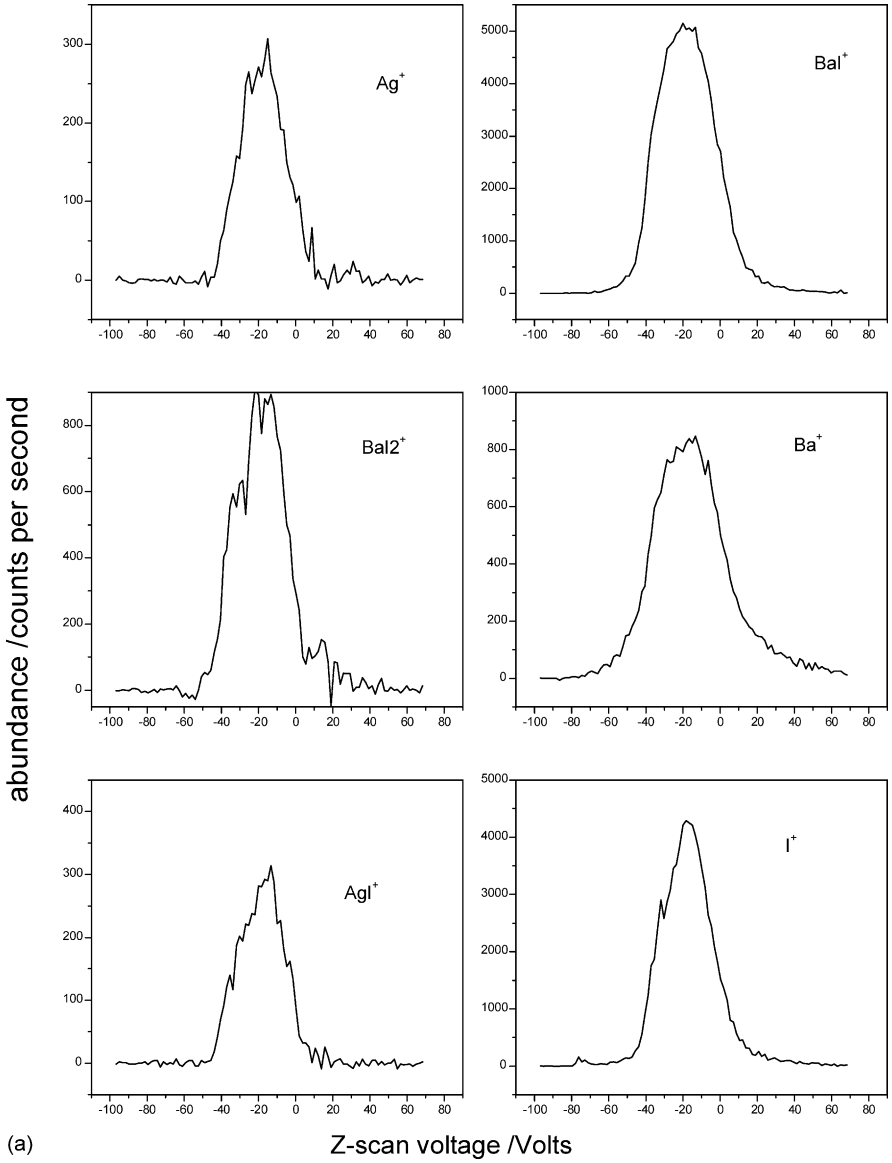

Fig. 6. (a) System BaI_2–Ag. Z-scans curves measured at 40 eV and 973 K. Due to the low pressures, a second accumulation was used for each experimental point in this case. The distribution of the iodine ion is narrower, proving that it is not a fragment of BaI_2. The existence of atomic iodine probably accounts for the AgI formation. (b) Relative ionisation cross-section curves for ions obtained from Ag–BaI_2 system at 820 K.

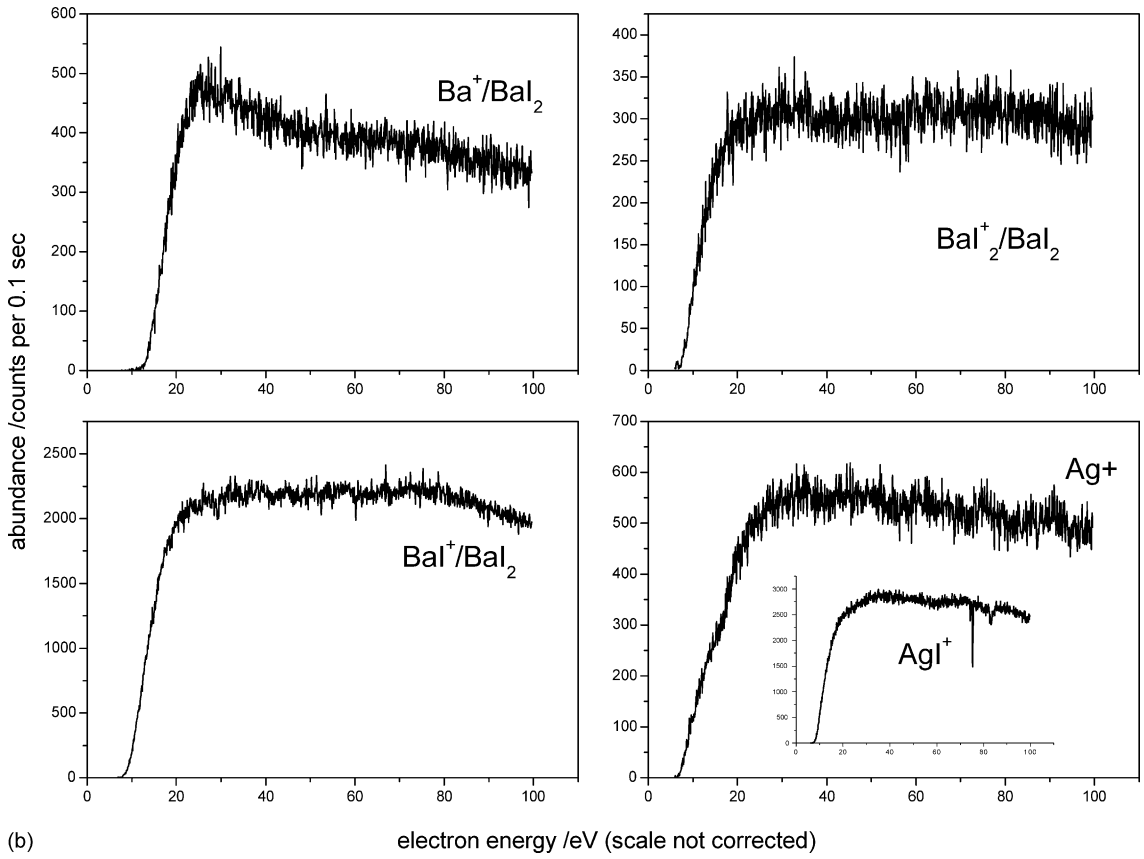

Fig. 6. (*Continued*).

a value of 9.06×10^{-18} cm^2 for the ionisation cross-section of BaO if area is considered. From this point the notation, σ will mean σ(max). Some lower value is obtained (7.46×10^{-16} cm^2) if ion intensities are considered. Prior to chemical analysis of the deposit, an auxiliary non-destructive method was applied in order to analyse the thin film deposit composition. The result of proton induced X-ray emission (PIXE) analysis differed from the subsequent chemical determination of the deposit (Au:Ba = 20:1 by weight), leading to a higher value for σ_{BaO} (13.4×10^{-16} cm^2). The first term of Eq. (3) represents the vapour pressure ratio (p_{Au}/p_{BaO}) at 1523 K, which is 11.96. Taking a value of 0.09904 Pa [16] for the vapour pressure of gold at 1523 K, we get 8.281×10^{-8} bar for the vapour pressure of BaO at 1523 K, agreeing with Hilpert and Gerads' [6] value (see Table 1) obtained in a more indirect way, through Ag–BaO cross-section consideration. Taking Mann's value of 5.84×10^{-16} cm^2 for σ_{Au} is an arbitrary choice. So far, no measured data for the absolute value of σ_{Au} exists. However, several measured values [22–25] for the (σ_{Au}/σ_{Cu}) ratio can be found, ranging from 0.5 [22] up to 2.1 [23], while the theoretical value of Mann [21] for this ratio is 1.5. It was therefore a straightforward decision, to confirm the latter value with a separate experiment. To accomplish this, an Au/Cu alloy (0.53/0.47) was additionally measured at 1523 K. Ten measurements were also performed resulting in Au/^{63}Cu ion abundance ratio of (3.82 ± 0.1). The ionisation cross-section curves of an Au/Cu system and *Z*-scan spectra (measured at 40 eV) are shown in Fig. 3a and b.

From the ICP-AES analysis of the deposit (18.5 μg Au, 3.5 μg Cu) and $\sigma_{Cu} = 4.09 \times 10^{-16}$ cm^2 (Freund et al.'s [26] experimental value) we obtain 5.2×10^{-16} cm^2 for σ_{Au}, which is close to Mann's value of 5.84×10^{-16} cm^2, and 1.274 is our experimental value for the (σ_{Au}/σ_{Cu}) ratio. PIXE determination of the Au/Cu deposit film showed better agreement with the ICP-AES analysis, resulting in 5.7×10^{-16} cm^2 for σ_{Au} and 1.38 for (σ_{Au}/σ_{Cu}). Using the average value of 5.45×10^{-16} cm^2 for σ_{Au}, we obtain 9.9×10^{-16} cm^2 for σ_{BaO}, based on Freund et al.'s [26] experimental result for σ_{Cu} (4.09×10^{-16} cm^2). However, Bolorizadeh et al. [27] consider Freund et al.'s [26] value for σ_{Cu} too high and a lower value of 3.21×10^{-16} cm^2 was obtained in the author's [27] own work. The reason for the criticism was on account, that the fast atomic beam of Cu in Freund's experiments contained a substantial admixture of metastable species whose effect on the measured cross-section 'is impossible to assess'. Due to rather significant differences in σ_{Cu} value (~25%) we decided to confirm Bolorizadeh's result by measuring a Ag0.05Cu0.95 alloy. To accomplish this, 50 mg of alloy was evaporated at 1373 K from a BN cell for 24 h. During evaporation, the (^{107}Ag/^{63}Cu) ratio was measured occasionally. The results

are shown in Fig. 4. Fig. 4 shows that the (^{107}Ag/^{63}Cu) ratio decreases with time due to the higher vapour pressure of Ag and its increased removal from the liquid alloy. The experimental points were further fitted to an exponential decay function, from which the average ratio could be calculated as 3.55 or 4.77 after isotope correction. The ICP-AES analysis found 2.8 μg of Ag and 0.8 μg of Cu in the deposited film. From these data, the (σ_{Ag}/σ_{Cu}) ratio was obtained as 1.776. Using Freund's value for $\sigma_{Ag} = 5.47 \times 10^{-16}$ cm^2 we get 3.08×10^{-16} cm^2 for σ_{Cu} which confirms the assumptions of Bolorizadeh et al. [27].

Thus, our result for σ_{BaO} (9.9×10^{-16} cm^2) must be considered as an upper limit, in agreement with the estimations of the authors [4,6,14] but still being in serious contradiction with the experimental results of Hastie et al. [8] and considerations in [7].

Certainly such a situation calls for a cross examination of some additional Ba compounds with the (MCM) model [7]. Barium difluoride and barium diiodide were selected as a appropriate compounds due to the high difference in ionisation cross-section of the two halogens, for which a classical approach of additivity suggests much higher sigma value for BaI_2 than for BaF_2.

3.1. BaF_2–Cu system

Copper was used as the reference material in case of the BaF_2 due to similar vapour pressure and that no Cu–F compounds were found in the mass spectrum during evaporation. The sample was evaporated at 1323 K for 45 h. Four runs were made, the results are shown in Tables 3a and 3b and Fig. 5a and b. In deposit 3.9 μg Cu and 8.6 μg Ba was found using ICP-AES. Applying Eq. (3) for the present case, we obtain 8.8×10^{-16} cm^2 for σ_{BaF_2} if the area is used for ion abundance or 6.8×10^{-16} cm^2 if ion intensities are considered. It is interesting to compare this result with the one obtained *via* the literature vapour pressures of BaF_2 and Cu. Taking both values from IVTANTHERMO [16] we get 3.2×10^{-16} cm^2 for σ_{BaF_2}. By using Pankratz's [28] pressure for BaF_2, 9.5×10^{-16} cm^2 can be obtained for σ_{BaF_2}, which agrees with our accepted value of 8.8×10^{-16} cm^2.

3.2. Ag–BaI_2 system

In the mass spectrum of a Ag–BaI_2 mixture, the AgI^+ ion was also detected in addition to Ag^+, BaI_2^+, BaI^+, Ba^+ and I^+. Due to its similar abundance to Ag^+, it was not possible to obtain an accurate Ag/BaI_2 ratio vapour pressure by chemical analysis of the deposited material, and the values were taken from IVTANTHERMO. It was also necessary to investigate the fragmentation pattern of pure AgI to make the necessary correction on Ag^+ ion due to Ag^+/AgI fragmentation process. AgI was probably formed by a direct reaction between Ag and iodine, rather than by an exchange reaction. To keep the abundance of AgI as low as possible we made measurements at the lowest possible temperature (973 K). In Fig. 6a, a typical *Z*-scan run is shown. At 973 K, the absolute vapour pressures of Ag and BaI_2 are 2.4×10^{-4} Pa and 4.3×10^{-3} Pa, respectively [16] and 18.2 is the ratio. The integrated area ratio, with isotope correction (see Fig. 6a) is 44.1. Here, no iodine ion was included in the summation since it is evident from its *Z*-scan shape that I^+ is not a fragment ion. Iodine is probably contained in BaI_2 and is at the same time responsible for the AgI formation. The area of Ag^+ was therefore corrected by subtraction of 50% (obtained from mass spectra of pure AgI) of the AgI^+ area. From these data and $\sigma_{Ag} = 5.47 \times 10^{-16}$ cm^2, the resulting ionisation cross-section of BaI_2 is 13.3×10^{-16} cm^2. A much lower value is obtained (9.1×10^{-16} cm^2) using ion intensities instead of areas. The shape of cross-section curves measured at 820 K are shown in Fig. 6b.

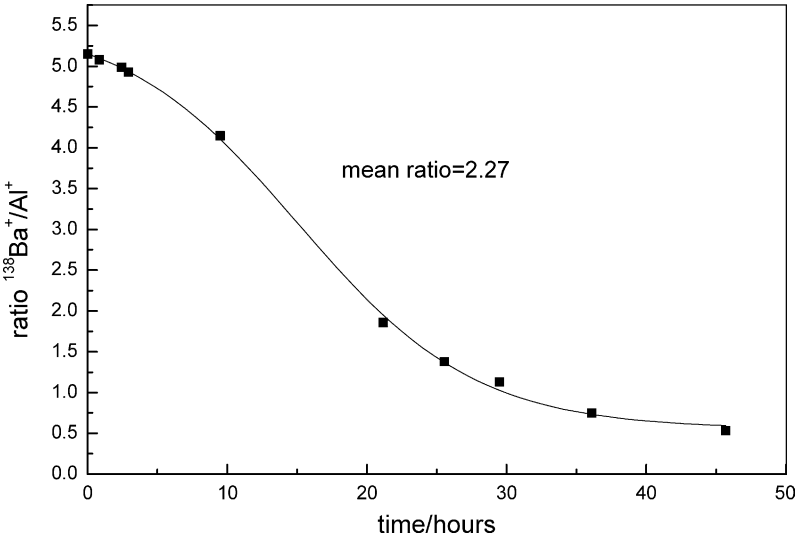

Fig. 7. $^{137}Ba^+/^{105}Ag^+$ ratio in variation with time. Average ratio is 2.27.

3.3. BaO–Al system

To measure the σ_{Ba}/σ_{Al} ratio, a mixture of BaO with the excess of Al was heated at 1253 K in a graphite Knudsen cell. Barium was generated through the following reaction:

$$3BaO(s) + 2Al(s) \rightarrow 3Ba(g) + Al_2O_3(s)$$

According to the IVTANTHERMO data, the equilibrium pressure of Ba for this reaction is 109 Pa which is 10,000 times higher than the equilibrium pressure of Al (0.01 Pa) at the specified temperature. The experimental ratio of ion currents ($^{138}Ba^+/Al^+$) was 5.15 at the beginning of evaporation and showed a decreasing tendency through 45 h of evaporation, see Fig. 7. The unexpected low Ba signal could be explained by the low BaO activity in the reaction mixture and/or the kinetic limitation of the reaction rate. The experimental points for Ba/Al ratio shown in Fig. 7 were fitted to sigmoidal function, from which the average ratio was calculated as 2.27. In the deposit, 165 μg Ba and 39 μg Al was found. The calculated maximum cross-section of Ba (at 24 eV), based on the Al cross-section at 24 eV (9.5×10^{-16} cm^2, Freund) is 16.04×10^{-16} cm^2, whereas the σ_{Ba}/σ_{Al} ratio is 1.69 at 24 eV. In Fig. 8, our measured cross-section curves for Al and Ba are shown together with Dettmann and Karstensen's [29] for Ba and Freund et al.'s [26] for Al. Also shown is the theoretical curve for Ba obtained from [21]. A perfect match is also noticed for the auto-ionisation structure of Ba at 19 and 24 eV. At higher energies, our curve decreases more slowly than in case of [29] which has already been noticed in our former work [30].

4. Reliability of measurements and sources of errors

The experimental approach used in this work completely eliminates systematic errors due to vapour pressure uncertainties. It also minimises errors concerning the discrimination of energetic fragment ions relative to molecular and/or atomic ions at the magnet slit (in *Z*-direction). It does not, however, eliminate the problems involving the extraction of energetic fragment ions from the ion source. In our recent study [30], the extraction efficiency was studied by SIMION for such ions. We found, that 30% ions with an average energy of 0.3 eV was lost, i.e., did not pass our ion source exit slit being as broad as 1 mm (in *Y*-direction). In the present work, no such analysis was done since the energy distribution of the fragment ions was not measured. Therefore, our results must be considered as the lower limit in the cases, where the fragment ions are of significant abundance (BaI_2, BaO and BaF_2). It should be pointed out again, that a simple intensity comparison between standard (Ag) and measured compound which fragments after ionisation is not an adequate procedure leading to erroneous pressures of a factor of two in case of BaF_2.

Another source of error in the present work (and KCMS measurements in general) is the difficulty in reproducing the correct shape of the ionisation curves by mass spectrometer. Either the maximum appears at an incorrect position or the decreasing trend after maximum is altered. It was a usual procedure in this work, that prior *Z*-scan measurements were run, the shapes of the ionisation cross-section curves of the standard were checked (compared with the literature). A typical example of this problem can be seen by

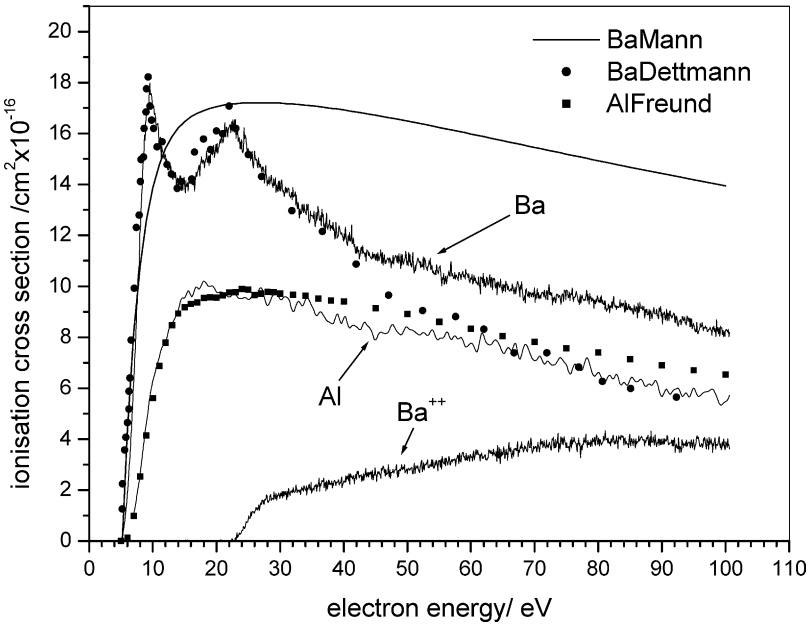

Fig. 8. Absolute ionisation cross-section of Ba, based on Freund's value of 9.5×10^{-16} cm^2 for Al at 24 eV. There is an excellent agreement for the absolute value as well as the shape to that published by Dettmann and Karstensen [29] from threshold to 40 eV. At higher energies, our curve shows less decreasing tendency.

comparing the shapes of the Au curves in Figs. 2b and 3b. They differ to some extent, introducing a certain degree of uncertainty to the final result. Also, the measured curve of Cu in Fig. 3b shows a steeper decrease than in the literature [26]. We consider this problem less important than the previous one, leading to uncertainties of less than 10% (in our case) for cross-section ratio with supposition that all ions are effected in a similar way.

The accuracy of chemical analysis (ICP-AES) as declared by analyst is better than ±5% [31]. A typical relative statistical error of the ion abundance ratio (see Tables 2a and 3a) is less than 5%, and 10% for the absolute abundance of separate ions. which, does not effect the overall error. We estimate the reliability of our results for cross-section ratios within 20%, exclusive of the uncertainties caused by ion extraction discrimination. In the case of BaI_2–Ag, our result depends on reliability of vapour pressure data used in the calculation.

5. Comparison of the measured cross-sections with MCM predictions

Application of Eq. (3) in [7] gives the BaO, BaF_2 and BaI_2 ionisation cross-section to be, 8.4, 6.9 and 15.1, respectively. These are in excellent agreement with our experimental values of 9.9 (5.8), 8.8 (6.6) and 13.3, respectively. The values in parenthesis refer to $\sigma_{Cu} = 3.08$ instead of 4.08. By considering 100% ionic character of the measured molecules, the MCM predicts much lower sigma values, 1.6, 2.2 and 10.1, respectively, not consistent with the experiment. This implies that BaO, BaF_2 and BaI_2 should all be treated as partly covalent molecules in MCM considerations. Also, the use of a classical atomic cross-section additivity approach should be corrected by at least for a factor of 0.5 and it was indeed a good choice of Hilpert and Gerads [6] to use 0.4 for σ_{Ag}/σ_{BaO} ratio at 22 eV.

6. Conclusion

A Knusden cell mass spectrometric experiments were made to measure the ionisation cross-sections of Ba, BaO, BaF_2 and BaI_2 using various internal standards. Vapour pressure ratios needed for calculations were obtained by analysing the Ba to standard concentration ratio in the cell effusate. The approach eliminates the errors originating from vapour pressure data. It also minimises the errors caused by the low transmission of fragment ions through the mass spectrometer. The reliability of the method was tested by measuring several metallic systems; Au/Cu, Ag/Cu and Al/Ba. In all cases our results for the cross-section ratio of those metals were found in consistency with the literature data [26,27,29], the overall systematic error being almost entirely dependent on the reliability of chemical analysis of the effusate. The results obtained for BaO, BaF_2 and BaI_2 cross-sections were in good agreement with predictions obtained by the MCM model of Hastie [7] provided that the partly covalent character of the measured molecules is considered.

Acknowledgements

The financial support of the Ministry of Education Science and Sport of Slovenia is gratefully acknowledged. The author also wishes to thank to Dr. Laszlo Bencze, Eötvös Lorand University, Budapest, for reviewing the manuscript and his critical comments. Thanks go also to Dr. Bojan Budič from the National Institute of Chemistry of Slovenia, for his effort in ICP-AES analyses.

References

[1] J.W. Otvos, D.P. Stevenson, J. Am. Chem. Soc. 78 (1956) 546.
[2] J.B. Mann, J. Chem. Phys. 46 (1967) 1646.
[3] R.F. Pottie, J. Chem. Phys. 44 (1966) 916.
[4] M.G. Inghram, W.A. Chupka, R.F. Porter, J. Chem. Phys. 24 (1955) 2159.
[5] M. Farber, R.D. Srivastava, High Temp. Sci. 7 (1975) 74.
[6] K. Hilpert, H. Gerads, High Temp. Sci. 7 (1975) 11.
[7] J.W. Hastie, A Predictive Ionization Cross-section Model for Inorganic Molecules, NISTIR 6768, 2001.
[8] J.W. Hastie, D.W. Bonnell, P.K. Schenck, Pure Appl. Chem. 72 (2000) 2111.
[9] A. Claassen, C.F. Veenemanns, Z. Phys. 80 (1933) 342.
[10] J.P. Blewett, H.A. Liebhafsky, E.F. Hennelly, J. Chem. Phys. 7 (1939) 478.
[11] R.S. Newbury, G.W. Barton Jr., A.W. Searcy, J. Chem. Phys. 18 (1968) 2793.
[12] G.A. Semenov, O.S. Popkov, A.I. Soloveichik, S.N. Parsiyaninova, Russ. J. Phys. Chem. 46 (6) (1972) 898.
[13] M.G. Inghram, W.A. Chupka, R.F. Potter, J. Chem. Phys. 24 (1955) 2159.
[14] M. Farber, R.D. Srivastava, High Temp. Sci. 7 (1975) 74.
[15] JANAF, Thermochemical Tables, 3rd ed., J. Phys. Chem., Ref. Data (1985) 14 Suppl.
[16] IVTANTHERMO, Database on thermodynamic properties of individual substances, Developed in Thermocentre of the Russian Academy of Science, Copyright © CRC Press, New York, 1993.
[17] C.B. Alcock, High Temp. High Pressures 20 (1988) 165.
[18] J. Drowart, in: J. Marsel (Ed.), Proceedings of the International School of Mass Spectrometry, Ljubljana, 1969.
[19] K. Stephan, H. Deutsch, T.D. Maerk, J. Chem. Phys. 83 (11) (1985) 5712.
[20] L.N. Gorokhov, N.E. Khandamirova, in: J.F.J. Todd (Ed.), Advances in Mass Spectrometry, Part B, 1985, p. 1031.
[21] J. Drowart, Technical Report, Pure Appl. Chem., in preparation.
[22] C.B. Alcock, High Temp. High Pressures 20 (1988) 165.
[23] J.M. Schroeer, D.H. Gunduz, S. Livingston, J. Chem. Phys. 58 (11) (1973) 5135.
[24] M. Ackerman, F.E. Stafford, J. Drowart, J. Chem. Phys. 33 (1960) 1784.
[25] M. Ackerman, J. Drowart, F.E. Stafford, G. Verhaegen, J. Chem. Phys. 36 (1962) 1557.

[26] R.S. Freund, R.C. Wetzel, R.J. Shul, T.R. Hayes, Phys. Rev. 41 (7) (1990) 3575.
[27] M.A. Bolorizadeh, C.J. Patton, M.B. Shah, H.B. Gilbody, J. Phys. B: At. Mol. Opt. Phys. 27 (1994) 175.
[28] L.B. Pankratz, Thermodynamic Properties of Halides, Bureau of Mines, 1984, Bulletin 674.
[29] J.M. Dettmann, F. Karstensen, J. Phys. B: At. Mol. Phys. 15 (1982) 287.
[30] A. Popovič, A. Lesar, J.V. Rau, L. Bencze, Rapid Commun. Mass. Spectrom. 15 (2001) 479.
[31] S. Klemenc, B. Budič, J. Zupan, Anal. Chim. Acta 389 (1–3) (1999) 141.